

Dynamics of fingering convection II: The formation of thermohaline staircases.

S. STELLMACH^{1,2,3}, A. TRAXLER²,
P. GARAUD², N. BRUMMELL²,
AND T. RADKO⁴

¹ Institut für Geophysik, Westfälische Wilhelms-Universität Münster, D-48149 Münster, Germany

² Applied Mathematics and Statistics, Baskin School of Engineering, University of California, Santa Cruz, CA 96064, USA

³ Institute of Geophysics and Planetary Physics, University of California, Santa Cruz, CA 96064, USA

⁴ Department of Oceanography, Naval Postgraduate School, Monterey, CA 93943, USA

(Received ?? and in revised form ??)

Regions of the ocean's thermocline unstable to salt fingering are often observed to host thermohaline staircases, stacks of deep well-mixed convective layers separated by thin stably-stratified interfaces. Decades after their discovery, however, their origin remains controversial. In this paper we use 3D direct numerical simulations to shed light on the problem. We study the evolution of an analogous double-diffusive system, starting from an initial statistically homogeneous fingering state and find that it spontaneously transforms into a layered state. By analysing our results in the light of the mean-field theory developed in Paper I, a clear picture of the sequence of events resulting in the staircase formation emerges. A collective instability of homogeneous fingering convection first excites a field of gravity waves, with a well-defined vertical wavelength. However, the waves saturate early through regular but localized breaking events, and are not directly responsible for the formation of the staircase. Meanwhile, slower-growing, horizontally invariant but vertically quasi-periodic γ -modes are also excited and grow according to the γ -instability mechanism. Our results suggest that the nonlinear interaction between these various mean-field modes of instability leads to the selection of one particular γ -mode as the staircase progenitor. Upon reaching a critical amplitude, this progenitor overturns into a fully-formed staircase. We conclude by extending the results of our simulations to real oceanic parameter values, and find that the progenitor γ -mode is expected to grow on a timescale of a few hours, and leads to the formation of a thermohaline staircase in about one day with an initial spacing of the order of one to two metres.

Key Words: Double Diffusive Convection, Geophysical Flows

1. Introduction

Fingering convection is a small-scale mixing process driven by a well-known double-diffusive instability of stably stratified fluids. When density depends on two components with opposite contributions to the overall stratification, a fingering instability may develop if the diffusivity of the stably stratified component is larger than the diffusivity

of the unstably stratified one. This commonly occurs in a large variety of natural environments, the best studied one being the heat-salt system in the oceanic thermocline (Schmitt 1994; Schmitt *et al.* 2005). Other areas of application range from the Earth’s atmosphere (Merceret 1977; Bois & Kubicki 2002) to magmatic melts (Tait & Jaupart 1989) and the interiors of giant planets (Guillot 1999) and stars (Vauclair 2004; Charbonnel & Zahn 2007; Stancliffe *et al.* 2007).

Scientific interest in the dynamics of fingering convection, the saturated state of the fingering instability, is twofold. When viewed as a small-scale turbulent process, it is an intrinsic source of diapycnal mixing in stably stratified regions, which operates even in the absence of mechanical forcing. As such, it can play an important role in controlling the global transport of heat and chemical species in the system considered (see reviews by Schmitt, 1995 and Ruddick & Gargett (2003)). Fingering convection is also known to drive dynamics on much larger scales by exciting a variety of secondary instabilities, such as internal gravity waves through the collective instability (Stern 1969; Stern *et al.* 2001), thermohaline intrusions (Stern 1967; Toole & Georgi 1981; Walsh & Ruddick 1995) and the more recently discovered γ -instability (Radko 2003). Generally speaking, these secondary instabilities are driven by a positive feedback mechanism between large-scale temperature and salinity perturbations, and the turbulent fingering fluxes induced by these perturbations. In Paper I, we provided definitive measurements of the small-scale turbulent fluxes induced by fingering convection in the heat-salt system, and unified all previous theories of the large-scale secondary instabilities in a single “mean-field” framework. In this paper, we now turn to one of the longest standing unsolved problems related to fingering convection, namely the formation of thermohaline staircases.

Thermohaline staircases are formed as stacks of deep convective layers, both thermally and compositionally well-mixed, separated by thin fingering interfaces. They are ubiquitously associated with active fingering convection, and have been observed both in laboratory experiments (Stern & Turner 1969; Krishnamurti 2003, 2009) and in oceanic field measurements (Tait & Howe 1971; Schmitt *et al.* 2005). Oceanic staircases are long-lived, and can span the entire thermocline, with individual layer heights ranging from 10m-100m and horizontal extents of km-size or more. Regions of the upper ocean which exhibit a staircase stratification have much larger diapycnal mixing rates compared with smoother regions supporting the same overall temperature and salinity contrasts (Schmitt *et al.* 2005; Veronis 2007). The layering phenomenon therefore needs to be understood to quantify its role in the overall transport balance in the ocean, and by extension, in many other systems as well.

Forty years after their original discovery, however, the mechanism responsible for the formation of thermohaline staircases essentially remains an enigma. Existing theories might be roughly classified into two groups. In a first class of models, layer formation is triggered by external effects in addition to fingering convection. It has been speculated for example that staircases and homogenous fingering both represent distinct metastable equilibria of the same system, and that layers are formed by external events which cause vigorous mechanical mixing and drive the system from one equilibrium to the other (Stern & Turner 1969). Since staircases are often observed in regions with significant lateral gradients of heat and salinity (such as the Mediterranean outflow for example), it has also been proposed that these gradients are actually required to trigger their formation, through the excitation and nonlinear evolution of the thermohaline intrusions (Walsh & Ruddick 1995; Merryfield 2000).

By contrast, a second class of ideas favour the notion that layering is inherent to the dynamics of fingering convection, with no need for external forcing. In these models, staircase formation is thought to arise from the nonlinear development of the two

other large-scale modes of instability mentioned earlier, namely the collective instability (Stern 1969; Stern *et al.* 2001) or the γ -instability (Radko 2003). Stern *et al.* (2001) studied the linear and nonlinear evolution of gravity waves excited by the collective instability, arguing that the overstable waves would eventually overturn and break into layers. However, while their numerical simulations show evidence for localized breaking events, these do not result in layer formation. Radko (2003) on the other hand put forward the γ -instability as the direct precursor of thermohaline staircases, since by nature the normal modes of this instability are vertically modulated but horizontally invariant perturbations in temperature and salinity. His two-dimensional direct numerical simulations (DNS), which are the first to exhibit unseeded spontaneous staircase formation from an initially homogeneous fingering field, appear to confirm his hypothesis.

Despite recent progress in this type of models, a number of fundamental questions remain to be addressed. The first relates to the validity of the mean-field framework: do the mean-field equations correctly model the large-scale dynamics of fingering systems? This question has so far only partially been answered for the linearised mean-field equations through idealised tests in which a single large-scale perturbation is seeded on the fingering field, its growth rate monitored and successfully compared with theoretical predictions (Stern *et al.* 2001; Radko 2003). However, whether such perturbations are indeed excited by the turbulence with a sufficiently large amplitude to rise above the noise level, and with sufficient scale separation for mean-field theory to be applicable, remains to be determined in the general case. Furthermore, we note that these tests have so far only been performed in two-dimensional numerical simulations. Given the well-known pathological nature of the energy transport from small to large scales in 2D turbulence (Kraichnan 1967), convincing validation of mean-field theory can only come from 3D simulations.

The second question is related to the problem of layer formation itself. Existing theories (Stern *et al.* 2001; Radko 2003) have each put forward a particular mean-field mode of instability as the precursor for staircase formation. As such, they consider each mechanism in isolation and ignore other possible unstable modes. In Paper I we identified the fastest growing modes, and showed that in the parameter regime where staircases are observed several kinds of mean field instabilities can simultaneously be excited. In fact modes on a considerable range of spatial scales, both direct and oscillatory in nature, are predicted to grow by mean field theory, and it seems likely that their mutual interaction disrupts their evolution. The resulting dynamics remains to be explored.

Finally, all previously proposed models assume that the nonlinear evolution of a mean-field mode eventually triggers the formation of layers. Unfortunately, the predictive power of these mean-field models breaks down as soon as turbulence on a wide and continuous range of spatial scales is generated. Three-dimensional computer simulations resolving all relevant scales currently are therefore the only way to study the final stages of layer formation.

The purpose of the present paper is to answer some of these questions, and ultimately illuminate the problem of staircase formation, via large-scale, three-dimensional numerical simulations of fingering convection. Since both small-scale fingers as well as deep layers have to be resolved simultaneously for this to be possible, and since fingers and staircases evolve on vastly disparate timescales, such simulations had until recently been impossible. Thanks to the rapid advances in high-performance computing, this is no longer the case.

Our paper is organised as follows. We begin by briefly summarising in Section 2 the basic equations for fingering convection, and describe our numerical model setup and selection of governing parameters. In Section 3 we present our results, the first large-scale

three-dimensional simulation showing spontaneous layer formation, which is fully resolved down to the dissipative scale. We analyse the simulation in the light of the mean-field theory presented in Paper I, focusing on the evolution of the various large-scale modes of linear instability. Our results enable us to place constraints on the applicability of mean-field theory, and lead to a clear and simple picture of the sequence of events finally resulting in layer formation. We conclude in Section 4 by summarising our results and by discussing their implications both in the oceanographic context, and further afield.

2. Equations and model setup

2.1. Governing equations

In natural systems, both fingering convection and staircase formation usually occur far from physical boundaries. It is therefore important to select a numerical setup which minimises boundary-effects. Following Stern *et al.* (2001) and Radko (2003), for example, we consider a fingering-unstable system, permanently forced by background vertical temperature and salinity gradients T_{0z} and S_{0z} . In this case, the non-dimensional model equations are:

$$\frac{1}{\text{Pr}} \left(\frac{\partial \mathbf{u}}{\partial t} + \mathbf{u} \cdot \nabla \mathbf{u} \right) = -\nabla p + (T - S)\hat{\mathbf{k}} + \nabla^2 \mathbf{u} , \quad (2.1a)$$

$$\nabla \cdot \mathbf{u} = 0 , \quad (2.1b)$$

$$\frac{\partial T}{\partial t} + w + \mathbf{u} \cdot \nabla T = \nabla^2 T , \quad (2.1c)$$

$$\frac{\partial S}{\partial t} + \frac{1}{R_0} w + \mathbf{u} \cdot \nabla S = \tau \nabla^2 S , \quad (2.1d)$$

where T denotes perturbations away from the linearly stratified background temperature, S the similarly defined salinity perturbation, p the pressure perturbation from hydrostatic balance, and the vector $\mathbf{u} = (u, v, w)$ is the velocity vector. The above system has been non-dimensionalised using the anticipated finger scale $d = (\kappa_T \nu / g \alpha T_{0z})^{1/4}$ (Stern 1960) as the lengthscale (where κ_T is the thermal diffusivity, ν the kinematic viscosity, g is gravity and α denotes the thermal expansion coefficient), and the thermal diffusion timescale across d , namely d^2 / κ_T , as the timescale. Temperature and salinity have been rescaled by $T_{0z}d$ and $\alpha T_{0z}d / \beta$ respectively, where β is the saline contraction coefficient. Three non-dimensional parameters control the behaviour of the system: the diffusivity ratio $\tau = \kappa_S / \kappa_T$, where κ_S is the salt diffusivity, the Prandtl number $\text{Pr} = \nu / \kappa_T$, and the background density ratio $R_0 = \alpha T_{0z} / \beta S_{0z}$.

To minimise the influence of boundaries, perturbations are assumed to be periodic in all three spatial dimensions. Hence for a computational domain of size (L_x, L_y, L_z) we set $q(x, y, z, t) = q(x + L_x, y, z, t) = q(x, y + L_y, z, t) = q(x, y, z + L_z, t)$ for $q \in \{T, S, \mathbf{u}\}$. This configuration guarantees in particular that layers cannot be generated artificially by flux convergence at solid boundaries (Özgökmen *et al.* 1998; Merryfield 2000). It is also important to note that the total horizontal averages of the temperature and salinity fields are not assumed nor forced to be zero, so that the mean vertical profiles of temperature and salinity can evolve freely with time.

Finally, note that by contrast with Paper I, we do not include lateral gradients, and thus suppress the mechanism driving intrusive modes. As such we restrict our analysis to spontaneously emerging staircases, and show how they may form even in the absence of any additional forcing. Although intrusions are important in regions of the ocean subject to very strong lateral gradients, this assumption is reasonable in more typical regions of

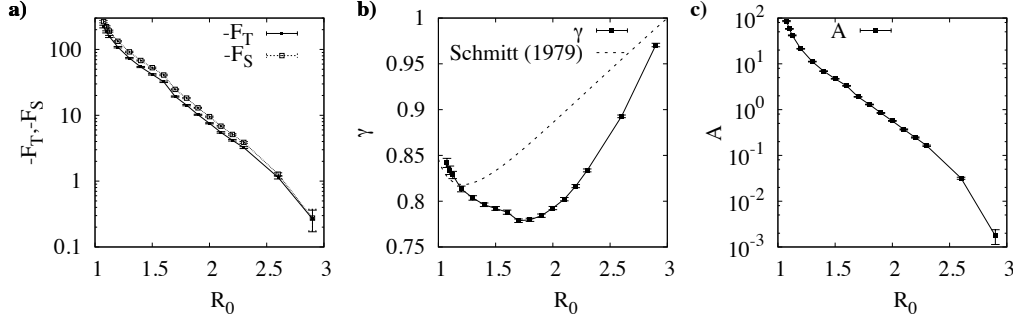


FIGURE 1. Numerically determined buoyancy fluxes due to heat and salt, $F_T = \langle wT \rangle$ and $F_S = \langle wS \rangle$ respectively, their ratio γ , and the Stern number $A = (F_S - F_T) / \text{Pr} (1 - 1/R_0)$, as a function of R_0 for $\tau = 1/3$ and $\text{Pr} = 7$. The theoretical prediction of Schmitt (1979) is shown in **b)** for reference. The fluxes were measured after integrating the model described in Section 2.1 to saturation, in a small domain of size $5 \times 5 \times 15$ fastest-growing finger widths (FGWs, see Schmitt (1979)). The experimental protocol for these measurements is similar to that described in the Appendix of Paper I. A necessary condition for the γ -instability (Radko 2003) is that $\gamma = F_T/F_S$ should be a decreasing function of R_0 . As shown in Figure 1b, this happens here when $R_0 < 1.7$. A necessary condition for the collective instability (Stern *et al.* 2001) is that the Stern number A should be larger than an order one factor. As seen in Figure 1c this condition is satisfied only for $R_0 < 1.7$ as well.

the thermocline since Paper I shows that for small-to-moderate lateral gradients, intrusive modes grow on much slower timescales than either gravity-wave modes or γ -modes.

2.2. Selection of the governing parameters

Simulations which have to resolve both fingers and possible larger scale structures such as thermohaline staircases still pose significant numerical challenges. As seen in Paper I (see Table 1), for parameter values appropriate for salty water ($\text{Pr} = 7$, $\tau \sim 0.01$), even a “small domain simulation” containing only a few fingers requires a resolution of the order of 1000^3 for low values of the density ratio to be fully resolved. Since our goal is to simulate a much larger domain, we are constrained to use a larger value of the diffusivity ratio instead, and choose $\tau = 1/3$. The Prandtl number on the other hand can be taken to be that of water ($\text{Pr} = 7$) without difficulty. Guided by Radko (2003), we adopt $R_0 = 1.1$ as the background density ratio.

As described in the introduction, we are interested in using the numerical simulation to study the causal relationship between the collective- and γ -instabilities and layer formation. Oceanic staircases are observed in regions with low density ratio, typically $R_0 < 1.8$ (e.g. Schmitt 1981). In this parameter regime, mean-field theory predicts that gravity-wave modes grow much more rapidly than γ -modes (see Figure 5 Paper I). We must then verify that our selected numerical parameter values $\text{Pr} = 7$, $\tau = 1/3$ and $R_0 = 1.1$ yield the same relative ordering of the growth rates of the various mean-field modes of instability. As shown in Paper I, these growth rates are solutions of a cubic equation where the coefficients of the cubic depend on the governing parameters (R_0 , Pr , τ), on the spatial structure of the mode, and on the functional dependence of the turbulent heat and salt fluxes on the density ratio. Using the methodology outlined in Paper I, we first measure these flux laws from small-domain experiments (Figure 1), and then use the results to calculate the growth rates of the mean-field modes (see Figure 2).

Figure 2 confirms that gravity-wave modes and γ -modes are both unstable in our numerical parameter regime, providing us with the opportunity to study them simul-

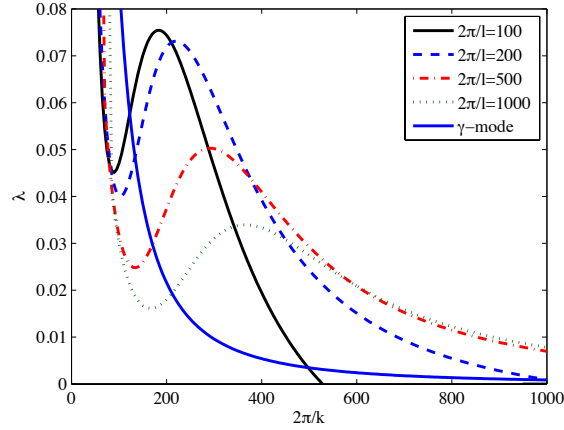


FIGURE 2. Growth rate λ of mean-field instabilities for $Pr = 7$, $\tau = 1/3$, and $R_0 = 1.1$, using the mean-field theory presented in Paper I and the flux laws presented in Figure 1. The horizontal axis represents the vertical wavelength in units of d , and the different curves represent different horizontal wavelengths as noted in the caption. Note that mean-field theory does not apply to structures which only contain a few individual fingers. This limits its validity to modes with horizontal and/or vertical wavelengths larger than about $100d$ (see Section 3.1 for detail).

taneously. Furthermore gravity waves are expected to dominate the system's behaviour while the γ -modes grow much more slowly. This choice of parameters thus guarantees that the basic properties of the unstable modes are comparable to those of the heat-salt system. Hence, despite the difference in parameters, we anticipate that our simulation should provide a reasonable view of the dynamics of real thermohaline staircase formation at $Pr = 7$, $\tau = 1/100$ and $R_0 \sim 1.5$.

2.3. Numerical considerations

Our large-scale simulation is performed in a domain of size $335d \times 335d \times 536d$, which corresponds to $27 \times 27 \times 43$ FGWs. The numerical algorithm for the solution of (2.1a-2.1d) with periodic boundary conditions is based on the standard Patterson-Orzag spectral algorithm and is presented in more detail in Paper I. Using small-domain tests to determine an adequate resolution for this parameter regime, we settled on a resolution of 576^3 equivalent grid points for the large-domain run. The computation was initialised with small amplitude white noise perturbations in the temperature and salinity fields, and evolved from $t = 0$ to $t = 900$ (in dimensionless time units). Note that the initial resolution was sufficient for most of the simulation but became inadequate in the layered regime, leading to a considerable accumulation of energy in the high vertical wave-number modes of the salinity field. Doubling the vertical resolution before layers start to form solved this problem: the results were interpolated to a $576 \times 576 \times 1152$ grid slightly *before* the layering transition and the simulation was then re-computed on the finer grid from there on.

3. Direct simulation of staircase formation

The dynamics of the system, as observed in our numerical simulation, are divided into three distinct phases illustrated in Figure 3. Note that a movie of this simulation is available in the online supplementary material. In Phase I, initial perturbations are amplified by the fingering instability, grow and eventually saturate into a state of vigorous

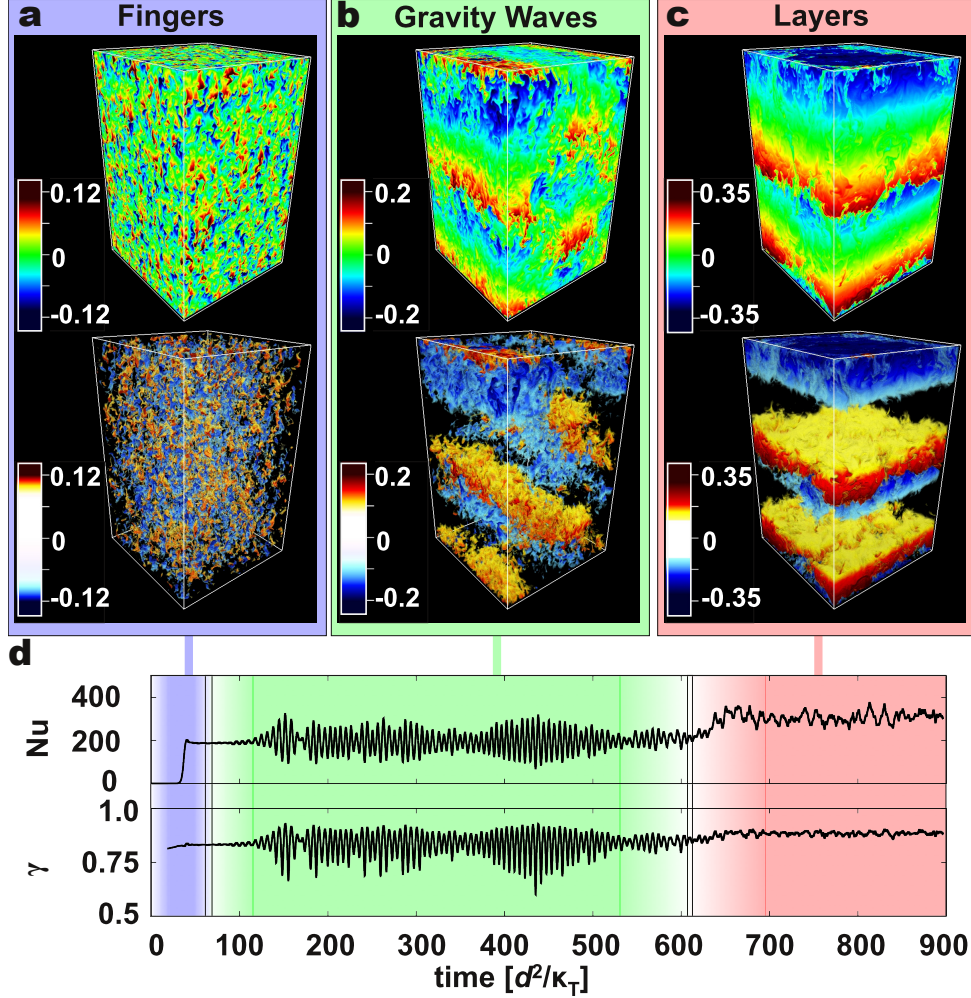


FIGURE 3. (a-c) Simulated layer formation in a large triply-periodic domain ($335d \times 335d \times 536d$). Temperature perturbations normalised to the temperature difference across the whole domain are shown in colour, with their respective colour scales in each panel. The top panels are visualisations on the data-cube faces, while the lower ones are volume-rendered images. Snapshots are shown for three characteristic dynamical phases. Fingering convection develops first (Phase I) and soon becomes unstable to large-scale gravity waves saturating at finite amplitude (Phase II). Eventually, vigorously convecting layers form, separated by thin fingering interfaces (Phase III). (d) Time-series of the Nusselt number $Nu = 1 - F_T$ and of the turbulent flux ratio $\gamma = F_T/F_S$.

fingering convection ($0 \leq t \leq 100$; Figure 3a). The global heat and salt fluxes, measured by $Nu = 1 - F_T$ and $\gamma = F_T/F_S$, are found to be identical to those determined previously in a smaller computational domain (see Figure 1a). However, the system does not remain in this homogeneous fingering state for long. Gravity waves rapidly emerge, grow and saturate (Phase II, for $100 \leq t \leq 600$), later followed by a sharp transition to a layered state (Phase III, $t > 600$). Phases II and III are now analysed in more detail.

3.1. Phase II : gravity-wave phase

Shortly after saturation of the fingering instability ($t \sim 100$), large-scale oscillatory modulations of the fingering field appear. They rapidly grow until $t = 150$ when they, in turn,

also saturate. We argue below that these modulations are large-scale finite amplitude gravity waves excited by the collective instability.

The visualisation of the temperature field presented in Figure 3b and in the online movie, for $t > 150$, reveals the presence of a dominant perturbation pattern, with a horizontal wavelength commensurate with the box width ($335d$), and a vertical wavelength half the box height ($268d$). Its temperature amplitude at saturation is of the order of 15% of the background temperature difference across the domain, and equivalently 30% of the temperature difference across one wavelength. The spatial pattern and relative amplitudes of the density and salinity perturbations are similar.

Figure 3d reveals that these large-scale perturbations strongly affect the global heat and salt fluxes. Both Nu and γ begin to show visible oscillations around their respective background values (i.e. as achieved in the homogeneous fingering state) shortly after $t = 100$, with increasingly larger amplitudes until saturation at about $t = 150$. By analogy with the effect of a pure gravity wave on global heat transport, we expect the Nusselt number to oscillate at twice the wave frequency, and similarly for γ . A power spectrum of the Nusselt number reveals a strong peak at $\omega \simeq 1.04$, so we estimate the wave frequency to be $\omega_g \simeq 0.52$. In our dimensionless units, the theoretical oscillation frequency for a pure gravity wave with phase planes inclined at an angle θ from the vertical is $\omega_g = \sqrt{\text{Pr}(1 - 1/R_0)} \cos \theta$, in other words $\omega_g = 0.8 \cos \theta$ for our selected parameter values. The dominant frequency observed is therefore compatible with the presence of a gravity wave with $\theta = 49^\circ$, which is consistent with our qualitative observation of the wave geometry. These results also confirm the theoretical prediction that gravity waves are the most rapidly growing mean-field mode in this parameter regime, and suggest that their absence from the 2D simulations of Radko (2003) is an artefact of reduced dimensionality[†].

We now study the gravity waves more quantitatively in the light of the linear mean-field stability analysis presented in Paper I. In this triply-periodic system, all mean-field modes have the normal form $\hat{q}_{lmk} \exp(ilx + imy + ikz)$ where \hat{q}_{lmk} is the mode amplitude, so that their predicted evolution can be compared straightforwardly with Fourier-transforms of the output of the simulation. Using this method, we extract from the numerical results the amplitude of each velocity component u , v and w , and compute the kinetic energy $E_{lmk} = (|\hat{u}_{lmk}|^2 + |\hat{v}_{lmk}|^2 + |\hat{w}_{lmk}|^2)/2$ of any mode with wave-vector $\mathbf{k} = (l, m, k)$, as a function of time. The results are shown in Figure 4.

For simplicity, in what follows, we use the notation $l_n = 2n\pi/L_x$, $m_n = 2n\pi/L_y$, as well as $k_n = 2n\pi/L_z$. Hence the dominant gravity-wave modes identified by eye in Figure 3b, which have one wavelength in the horizontal direction and two in the vertical direction, are denoted by $\mathbf{k} = (l_1, 0, k_2)$ or $\mathbf{k} = (0, m_1, k_2)$. Figure 4 shows that this set of modes, identified by a star symbol, begins to grow exponentially as soon as the background fingering convection reaches a saturated state. By $t = 200$, their kinetic energy is ten times larger than any of the other modes. Comparison of the observed growth rate with mean-field theory shows reasonable agreement from $t = 50$ to $t = 150$, although is slower than predicted by about 30%.

It is interesting to note that this dominant set of modes is not the most rapidly growing one according to linear theory: as seen in Figure 4, a variety of other gravity-wave modes have equal or larger predicted growth rates, as for example $\mathbf{k} = (l_2, 0, k_3)$. However,

[†] The difference in the wave dynamics in 2D and 3D may be attributed to the stronger negative feedback of the wave shear on salt fingers in 2D. In three dimensions, salt fingers tend to align into salt sheets parallel to the shear flow, which only moderately affects their vertical transport. In 2D such alignment is geometrically impossible and therefore adverse effects of shear on salt-fingers, and thus on the collective instability, are more profound.

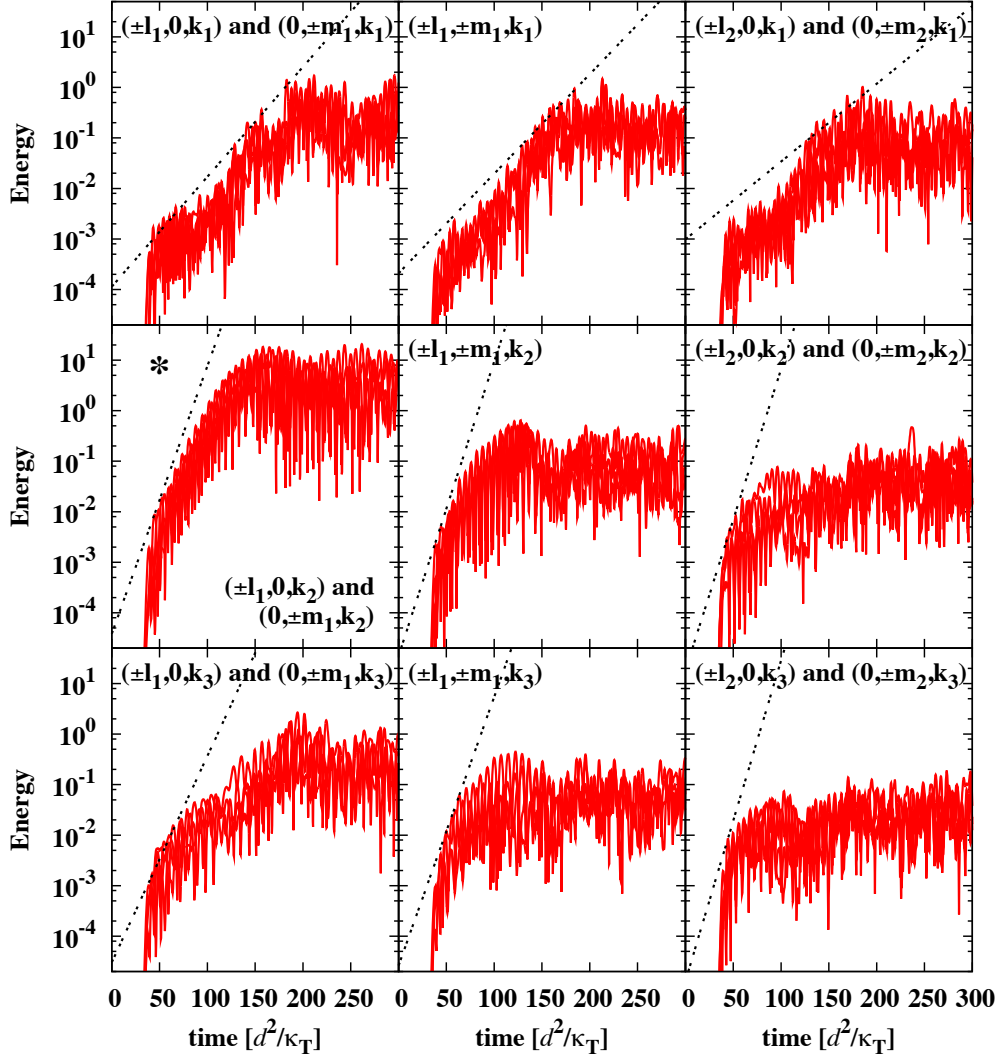


FIGURE 4. Kinetic energy in the first nine quartets of gravity wave modes, compared with the growth rate predicted using the mean-field theory presented in Paper I. Owing to the horizontal symmetry of the problem, modes $(\pm l, \pm m, k)$ and $(\pm m, \pm l, k)$ all have the same predicted growth rate, and are superimposed in each panel. The vertical wavenumber increases from top to bottom and the horizontal wavenumber increases from left to right. The $(\pm l_1, 0, k_2)$ and $(0, \pm m_1, k_2)$ modes (denoted by a star) are the “dominant modes” referred to in the main text.

not all modes grow as predicted. A systematic comparison between the observed and predicted growth rates of all nine sets of modes shown in Figure 4 reveals that mean-field theory becomes progressively less accurate with increasing wavenumber. This information is summarised in Figure 5. Since for our selected set of parameters a finger is typically 1 FGW wide and 5 FGW high (see Paper I), and $1\text{FGW} \sim 13d$, our results suggest that modes grow as predicted only if their horizontal extent is wider than about 10 fingers and their vertical extent is larger than about 5 fingers. Modes with intermediate horizontal or vertical extent still grow but slower than expected. Modes which only contain 3 or fewer fingers (horizontally or vertically) do not grow at all. These results are not surprising

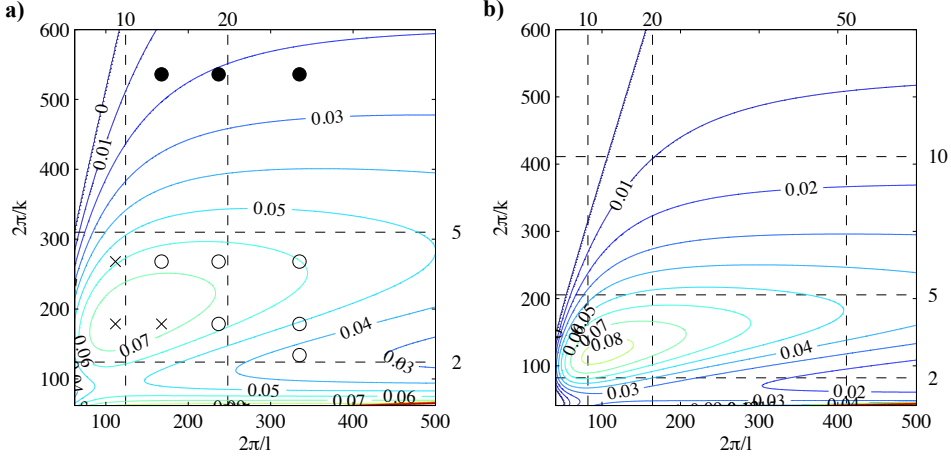


FIGURE 5. Contour plot of the growth rate of mean-field modes for a) our selected parameters $Pr = 7$, $\tau = 1/3$, $R_0 = 1.1$ and b) the heat/salt case $Pr = 7$, $\tau = 1/100$ with $R_0 = 1.5$. The individual modes presented in Figure 4 are identified on the left plot by symbols, showing modes which grow with the expected growth rates as filled dots, modes which grow but more slowly than expected as empty dots, and modes which do not grow at all as crosses. The individual modes, from top to bottom, have $k = k_1$, $k = k_2$, $k = k_3$, and $k = k_4$, and from right to left, have $(l = l_1, m = 0)$, $(l = l_1, m = m_1)$, $(l = l_2, m = 0)$, $(l = l_3, m = 0)$ and $(l = l_4, m = 0)$. The horizontal and vertical lines show the size of the structures considered in terms of finger widths and heights (taking, as shown in Paper I, that fingers are about 1 FGW wide and 5 FGW tall). The equivalent plot for the heat/salt system shown on the right, which was obtained by using the turbulent flux laws presented in Paper I, is very similar when viewed in terms of finger sizes.

given that separation between the mode scale and the individual finger scale is required for mean-field theory to be applicable. Note that, when viewed in terms of finger sizes, the growth rate plot for the heat/salt case at $R_0 = 1.5$, shown in figure 5b), is very similar to the one obtained for $\tau = 1/3$. It therefore seems reasonable to expect that finger driven oceanic gravity waves will also occur on length scales larger than the predicted fastest growing mean-field modes.

Finally, Figure 4 also reveals that all gravity-wave modes stop growing roughly at the same time, around $t \sim 150 - 200$. We now show that this is due to localised overturning events which are regularly triggered when some of the dominant modes constructively interfere to produce very high amplitude perturbations in the density field.

A single gravity-wave mode with vertical wavenumber k causes quasi-periodic oscillations of the total density field (background + perturbations). As the mode amplitude $\hat{\rho}_{l,m,k}$ grows, localised regions are progressively more weakly stratified. They become unstable to direct overturning convection when the perturbation reaches the critical value $\hat{\rho}_{l,m,k} = (1 - 1/R_0)/k$. Figure 6a compares the spectral power in the density perturbation of one of the four dominant modes – defined as the norm of the relevant coefficient of the Fourier transform of the density field – with the square of the critical amplitude for overturning. For this single mode, the criterion for overturn is clearly never reached. However, four of these dominant modes co-exist and can interact constructively to cause a localised overturning event. This effect is demonstrated in Figure 6b, which shows the filling factor of large-scale regions with positive density gradient, or in other words the relative volume of regions unstable to overturning convection. As expected, this filling factor is close to zero in the homogeneous fingering phase. It then rapidly increases to a few percent around $t = 150$, which corresponds to the time when the density spectral

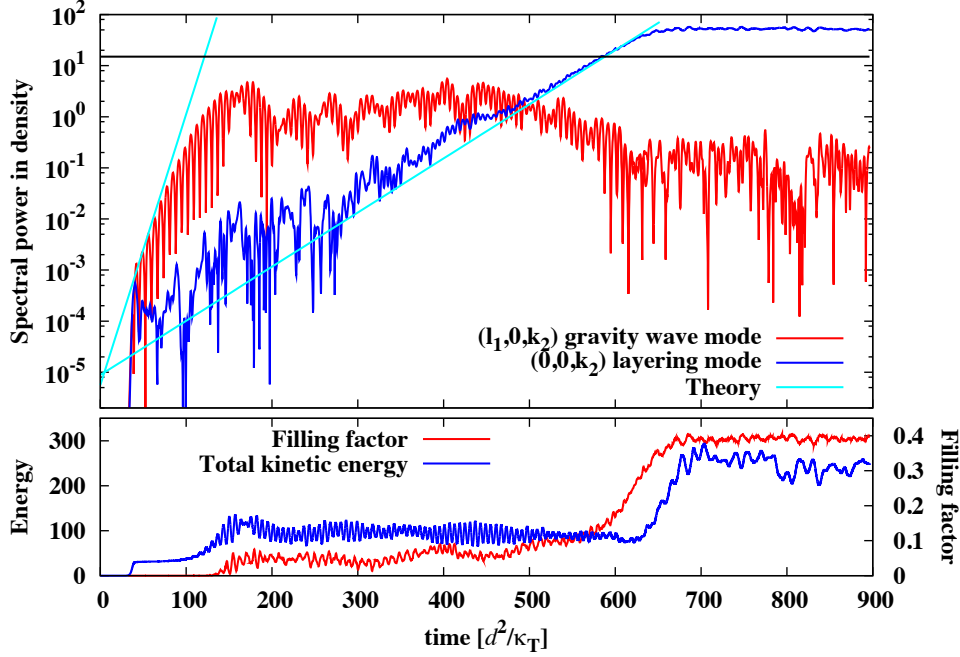


FIGURE 6. Top: Temporal evolution of one of the dominant gravity-wave modes $((l_1, 0, k_2))$, with horizontal wavelength $335d$, vertical wavelength $236d$ and of the $(0, 0, k_2)$ γ -mode (vertical wavelength: $236d$) respectively, as simulated numerically and as predicted by mean-field theory (Paper I). Shown is the norm of the Fourier coefficient of the density perturbation (the density spectral power). While the gravity-wave mode rapidly saturates the γ -mode slowly but steadily grows up to the critical amplitude for overturning (black line). Bottom: Filling factor of convectively unstable regions ($d\rho/dz > 0$), and total kinetic energy of the system. Note that in order to eliminate finger-scale density inversions, the filling factor is obtained from a low-pass filtered density field.

power of one of the dominant gravity-wave modes reaches about a tenth of the critical amplitude for overturning. After $t = 150$, the steady conversion of kinetic energy into potential energy by the localised and intermittent overturning events causes *all* the gravity-wave modes to stop growing and not just the dominant ones (see Figure 4). This result is not surprising given the nonlinear nature of the breaking events.

Our results show that the gravity wave-field saturates at fairly high amplitude, but *without directly triggering the formation of thermohaline layers*. The gravity-wave-dominated phase continues on for many more oscillation periods (from $t \sim 200$ to $t \sim 600$) and the movie of the simulations (see online material) shows no obvious visible change in the statistical properties of the flows. Our simulations show that the collective instability, as was originally proposed, does not appear to be responsible for the transition to the layered state observed in Phase III.

3.2. Phase III : Layered phase

The gravity-waves dominated phase suddenly ends around $t \sim 600$, with the spontaneous emergence of two convecting layers separated by thin fingering interfaces (Figure 3c). This layering transition is accompanied by a significant increase in the global heat and salinity fluxes (Figure 3d), as well as in the total kinetic energy (Figure 6). Figure 7

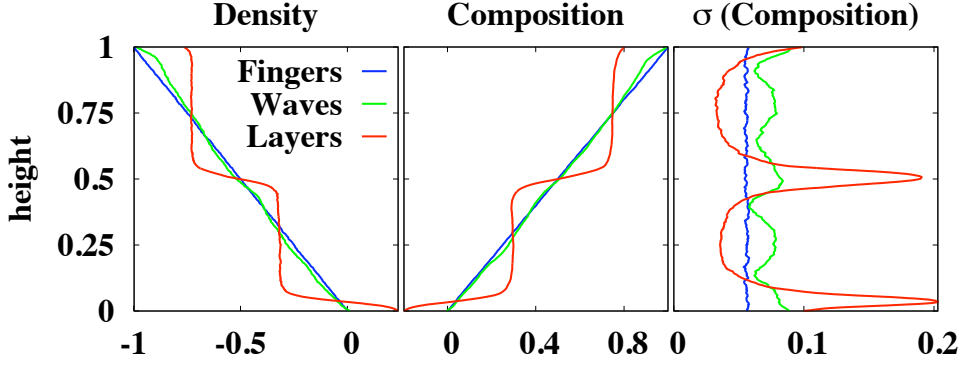


FIGURE 7. Horizontally averaged total density and salinity (in both cases, background + perturbation) and standard deviation of salinity $\sigma(S)$. Density and salinity are normalised by the respective background contrast over the entire domain, and height is given in units of the domain height. The three lines correspond to the visualisations in Figure 3. In the fingering phase, the salinity and density profiles are indistinguishable from the background profiles, and the standard deviation of salinity is statistically homogeneous. In the gravity-wave phase, the profiles remain close to the background profiles, but the presence of a $(0, 0, k_4)$ γ -mode can be seen in the $\sigma(S)$ profile. The layered phase exhibits a clear staircase in the salinity and density profiles, while $\sigma(S)$ shows strong peaks corresponding to the position of the fingering interfaces.

shows the resulting staircase in the mean profiles: turbulent mixing leads to a nearly homogeneous temperature and composition in the bulk of the layers, while the strongly-stratified interfaces exhibit larger spatio-temporal fluctuations in the temperature and salinity (as measured by the standard deviation from the mean) caused by the remaining fingering. The staircase, once formed, is extremely robust and persists despite being occasionally pierced by strong convective plumes.

3.3. The γ -instability and the formation of thermohaline staircases

In order to understand what causes the layering transition, we now study Phase II again in the light of predictions from mean-field theory. This time, we focus on the γ -modes discussed in Paper I and in Section 1. By virtue of being horizontally invariant and vertically periodic, γ -modes might straightforwardly overturn into a fully-formed thermohaline staircase once they reach the same critical amplitude as the one discussed in the context of gravity-wave modes above (see Section 3.1).

Since the emergent staircase in our 3D simulation has two layers, we naturally begin by studying the $(0, 0, k_2)$ γ -mode. Figure 6 shows that the $(0, 0, k_2)$ mode is indeed present in the simulation, and began to grow at the same time ($t \sim 50 - 100$) as the gravity waves studied above. Remarkably, we find that its growth rate is well modelled by linear mean-field theory all the way to about $t = 600$, even though the mean field approach does not account for the turbulent mixing induced by the overturning waves. This result establishes the predictive power of our formalism.

Figure 6 shows that this γ -mode reaches the critical amplitude for the onset of convective overturning at $t \sim 580$ and stops growing shortly thereafter when a regular staircase in the density (or temperature and salinity) profile appears ($t \sim 600$). The layers rapidly become fully convective, as can be seen in the strong increase in the filling factor of convectively unstable regions and of the total kinetic energy (see Figure 6), and the corresponding increase of the Nusselt number (see Figure 3d). Finally, note that the gravity

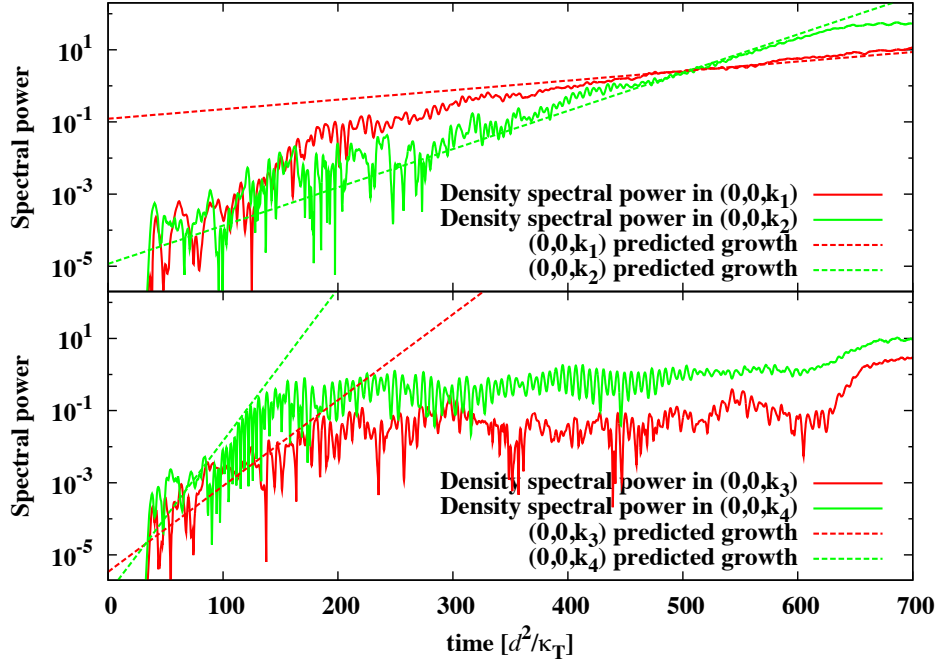


FIGURE 8. Density spectral power in the four largest vertical modes (with respective vertical wavenumbers k_1, k_2, k_3 and k_4), compared with mean-field theory. The two gravest modes (top panel) continue growing throughout the gravity-wave-dominated phase, while the other two modes (lower panel) stop growing around $t \simeq 150 - 200$.

waves can no longer exist in the layered state. Their amplitudes are strongly reduced, and stop showing a clear oscillatory signal.

3.4. The interaction of γ -modes and gravity-wave modes

The formation of thermohaline staircases in our simulation thus appears to depend only on the growth and eventual convective overturning of γ -modes, in a way which can be understood quantitatively using the mean-field theory and small-scale flux laws presented in Paper I and in Figure 1. In many ways, the fact that mean-field theory holds for the staircase progenitor, the $(0, 0, k_2)$ γ -mode, is rather remarkable given the presence of the strong gravity wave field, and deserves further attention. Moreover, as shown by Radko (2003), the γ -instability suffers from an ultra-violet catastrophe whereby the mode growth rates increase quadratically with wavenumber. As a result, the $(0, 0, k_2)$ γ -mode is not the most rapidly growing one according to linear theory, and one may wonder what led to its selection as the staircase progenitor.

To answer these questions, we begin by extracting information on other γ -modes in the system, with vertical wavenumbers ranging from k_1 to k_4 (modes with higher wavenumbers, as discussed earlier, are poorly represented by mean-field theory). Their temporal evolution is shown in Figure 8 and compared with theoretical expectations. As expected, the $(0, 0, k_4)$ mode grows the fastest among the ones studied, followed by $(0, 0, k_3)$, $(0, 0, k_2)$ and finally $(0, 0, k_1)$. At early times ($t < 200$), we see that the measured growth rates are indeed close to the corresponding theoretical ones for all modes except for $(0, 0, k_1)$, which unexpectedly grows significantly faster than predicted – the origin of this discrepancy remains a puzzle.

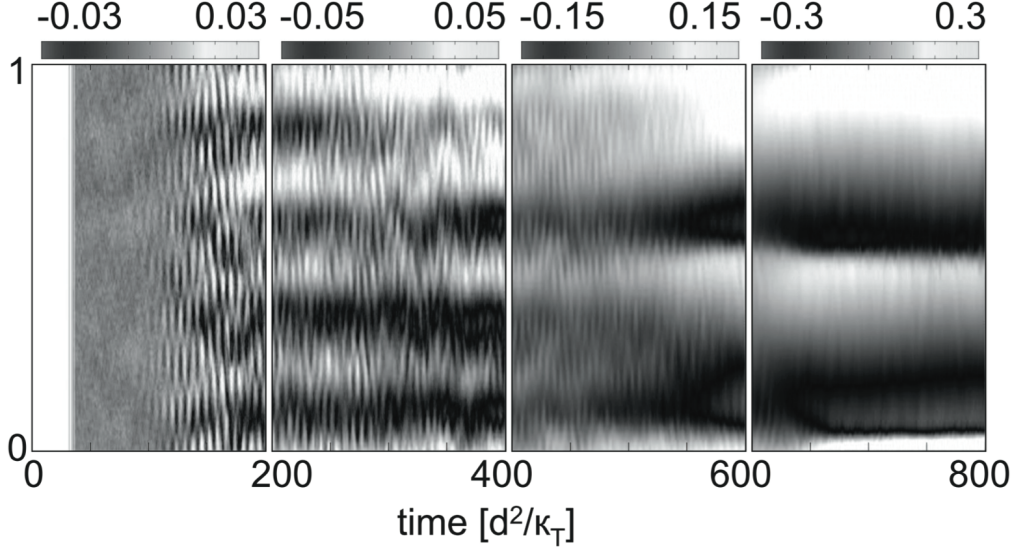


FIGURE 9. Horizontally averaged density perturbation $\langle \rho \rangle_h(z, t)$ as a function of time from $t = 0$ to $t = 800$. Four intervals are shown, each on a different colour scale to provide adequate contrast. From $t = 0$ to $t = 100$, mean perturbations to the background density are close to zero. However, notably regular oscillations appear around $t = 100$, with a k_4 vertical wavenumber and twice the temporal frequency of the dominant gravity-wave mode. By $t = 200$, the system shows clear evidence for the presence of a $(0, 0, k_4)$ γ -mode, strongly modulated by the gravity-wave field. Around $t = 500$, the $(0, 0, k_2)$ mode emerges as the dominant mode, continues to grow and begins to overturn around $t = 600$ into two mixed layers separated by sharp interfaces.

The subsequent evolution of the modes, beyond $t = 200$ in Figure 8, reveals an interesting dichotomy between the two larger-scale modes (top panel) which both grow with the expected growth rate, and the two smaller-scale modes (lower panel) which stop growing at about $t = 150 - 200$, when the gravity waves saturate. The amplitude of the $(0, 0, k_4)$ mode remains the largest one until about $t = 500$, even though it stopped growing at early times. Had it continued growing only slightly further, this mode would have been the one to cause the staircase formation, resulting in an initial layer height half of the one observed in the simulation. The evolution of the horizontally averaged density perturbation (denoted as $\langle \rho \rangle_h(z, t)$ from here on) shown in Figure 9 confirms more visually the dominance of the $(0, 0, k_4)$ mode until about $t = 500$, and the transition to a $(0, 0, k_2)$ mode thereafter (with a hint of $(0, 0, k_1)$ inducing a small asymmetry between the two layers).

The results of Figure 8 naturally prompt us to wonder why the smaller-scale modes stop growing during the gravity-wave phase while the larger-scale, slower growing modes do not. This important question impinges on the problem of the selection of the γ -mode which eventually becomes the staircase progenitor, and thus determines the initial layer spacing. In order to proceed further and understand what may cause the smaller-scale modes to stop growing, we need to gain further insight on the nonlinear dynamics of the various mean-field modes.

We can identify the dominant nonlinear mechanism for interaction between the various mean-field modes with a closer inspection of the $\langle \rho \rangle_h(z, t)$ profile. Figure 9 reveals notably regular oscillations from $t = 100$ to $t = 600$ which can be traced back to the nonlinear buoyancy transport induced by the dominant gravity-wave modes studied in Section 3.1. Indeed, a gravity-wave with vertical wavenumber k and frequency ω_g induces a

horizontally averaged vertical heat (or salt) flux $\langle wT \rangle$ or $\langle wS \rangle$ proportional to $\exp(2ikz + 2i\omega_g t)$. Since the dominant gravity-wave mode has a k_2 vertical wavenumber, the induced perturbations in $\langle \rho \rangle_h$ are expected to have a k_4 wavenumber and to oscillate at twice the wave frequency. This oscillation is indeed observed, and is most regular *before* the wave-breaking events begin, between $t = 100$ and $t = 150$ in Figure 9.

By virtue of being a quadratic quantity in the wave amplitude, the wave-induced flux is neglected in any standard linear mean-field theory. However, Figure 9 shows that it remains important throughout the entire wave-dominated phase from $t = 100$ to $t = 600$. In particular, it is responsible for the oscillations which are seen to modulate the $(0, 0, k_4)$ γ -mode rather strongly, either enhancing it or suppressing it depending on the phase of the wave. One may therefore conjecture that the $(0, 0, k_4)$ (and presumably the $(0, 0, k_3)$) γ -modes stop growing as a result of nonlinear interactions with the dominant gravity-wave modes through the wave-induced flux. Unfortunately, a complete quantitative understanding of the numerical results from our simulations, in particular in view of answering the question raised above, can only be gained from a thorough nonlinear analysis of our mean-field equations, a problem which is beyond the scope of the current paper. However, given that the dominant gravity-wave mode induces horizontally averaged fluxes with exactly the same vertical structure as that of the $(0, 0, k_4)$ γ -mode, the conjecture seems reasonable.

The question then remains of why the $(0, 0, k_2)$ and $(0, 0, k_1)$ γ -modes on the other hand still grow at the predicted rate despite the effect of the wave-induced flux. This result is even more remarkable for the $(0, 0, k_2)$ mode, which has an amplitude several orders of magnitude smaller than that of the dominant gravity-wave modes at early times. Again, without a full analysis of the nonlinear mean-field equations we are left to speculate on the matter. A plausible answer lies in the spatial mismatch between the small-scale flux modulation induced by the waves (working on the k_4 lengthscale) and the intrinsically larger scale of the two gravest γ -modes. However, showing this would again require a weakly nonlinear analysis of the mean-field equations, and is deferred to future work.

The results of the simulations, however, stand beyond the speculations. Whatever the cause for this observed effect, it appears that the dominant gravity waves act as a “filter” for any γ -mode with significantly smaller vertical wavelength. If we generalize this result to other parameter regimes, the progenitor of the staircase is always likely to be a γ -mode with wavenumber commensurate with that of the dominant gravity waves excited by the collective instability. As such, it is interesting to note that both sets of modes play a role in the eventual formation of a thermohaline staircase, although in a way which was neither anticipated by Stern (1969), nor by Radko (2003).

4. Discussion and prospects

Our simulation, when combined with the results of mean-field theory derived in Paper I, presents a clear and simple view of the sequence of events which may lead to the spontaneous formation of oceanic staircases (in the absence of lateral gradients or other sources of mechanical mixing), and which can also be straightforwardly generalised to other double-diffusive systems.

Let us first consider a homogeneous heat-salt system, with constant background temperature and salinity gradients unstable to fingering convection. At low enough density ratio ($R_0 < 4$, see Paper I), the turbulent flux ratio γ induced by fingering convection decreases most rapidly with R_0 . This regime is simultaneously unstable to two types of secondary large-scale “mean-field” instabilities: the collective instability which ex-

cites gravity waves (Stern 1969; Stern *et al.* 2001), and the γ -instability which leads to the growth of horizontally-invariant perturbations in the temperature and salinity field (Radko 2003).

As shown in Paper I, mean-field theory predicts that gravity-wave modes grow more rapidly than γ -modes for values of R_0 characteristic of regions of the ocean where thermohaline staircases are observed (i.e. $1 < R_0 < 1.8$). By comparison with numerical simulations at $Pr = 7$ and $\tau = 1/3$ we also found that the theoretically fastest-growing gravity-wave modes are actually too small for mean-field theory to be applicable. Instead, the emerging dominant gravity-wave modes are slightly more extended and have smaller theoretical growth rates. If we extrapolate the results of Figure 5a to parameter regimes relevant of the heat-salt system (see 5b), taking $R_0 = 1.5$ as a typical value for staircase regions, we find that the overall picture is very similar: modes which are large enough to grow with the theoretically predicted rate are very slowly growing modes, while the theoretically fastest growing ones are too small for mean-field theory to be applicable. As a result, we expect the dominant gravity-wave modes in the heat-salt system to be intermediate in size (20-30 fingers in width and 4-5 fingers in height), and grow with a non-dimensional growth rate of the order of about 0.04-0.05, taking into account that their real growth rate is expected to be smaller than the theoretically predicted one. Putting these results in dimensional form, using typical oceanic values of $\nu = 10^{-6} \text{m}^2 \text{s}^{-1}$, $\kappa_T = 1.4 \times 10^{-7} \text{m}^2 \text{s}^{-1}$, $\alpha_T = 2 \times 10^{-4} \text{K}^{-1}$, $g = 10 \text{ms}^{-2}$ and $T_{0z} = 10^{-2} \text{Km}^{-1}$, we have $d \sim 0.9 \text{ cm}$ and $1\text{FGW} = 8.2d$, so that a typical finger is of the order of 7 cm wide and 35 cm high. Hence the gravity waves expected to dominate the dynamics have horizontal and vertical wavelengths of the order of 1.5m - 2m, and grow on a timescale of the order of a few (3-5) hours.

These gravity waves saturate rapidly as a result of localised breaking events, without directly inducing layer formation. Meanwhile, a spectrum of γ -modes also grow, with one of them destined to become the progenitor of the thermohaline staircase. Our results suggest that the dominant gravity-wave modes interact nonlinearly with the γ -modes and act as a filter for the smaller-scale ones. Only those with vertical wavelengths larger than that of the dominant gravity-wave modes are allowed to grow, but then appear to do so on a timescale well-predicted by mean-field theory. Since the fastest growing γ -modes are those with the smallest vertical wavelength, we expect the progenitor of the staircase to be a mode with vertical spacing commensurate with the vertical wavelength of the dominant gravity-wave modes, i.e. around 5 fingers in height or about 1.5m-2m for parameters appropriate of the heat-salt system. This mode grows on a timescale of 5-6 hours, and upon reaching a critical amplitude, causes regularly-spaced inversions in the mean density profile which are subject to direct overturning convection. A regular staircase then forms, with an initial layer spacing of about 2m. Note that once formed, experiments (Krishnamurti 2003) and theory (Radko 2003, 2005, 2007) suggest that the staircase evolves further in time through successive mergers until an equilibrium layer depth is established. These events have not been observed in our 3D simulations yet since integrating the simulation on a merger timescale (Radko 2005) is numerically prohibitive in 3D.

Beyond giving new insight into the origin of oceanic staircases, our study marks a starting point in answering the question of whether gravity modes and γ -modes can be excited in other less readily observable fluid systems as well, and whether staircases may be expected or not. For example, it has been pointed out that vigorous fingering convection might occur in stars (Vauclair 2004; Charbonnel & Zahn 2007; Stancliffe *et al.* 2007), where the resulting transport may account for observed peculiarities in luminosity or metallicity. Our work suggests that, despite the complexity of these highly nonlinear

processes, much can still be learned first by obtaining local flux laws for turbulent mixing in the parameter regimes typical of these systems, and then applying the mean-field theory framework as show in Paper I and in this work.

A.T., P.G. and T.R. are supported by the National Science Foundation, NSF-093379, and T.R. is supported by an NSF CAREER. S.S. was supported by grants from the NASA Solar and Heliospheric Program (NNG05GG69G,NNG06GD44G,NNX07A2749). The simulations were partially run on the Pleiades supercomputer at UCSC, purchased using an NSF-MRI grant. Computing time was also provided by the John von Neuman Institute for Computing. We thank Gary Glatzmaier for many helpful discussions and for his continuous support.

REFERENCES

- BOIS, P.A. & KUBICKI, A. 2002 Double diffusive aspects of the convection in moist-saturated air. In *Continuum Thermomechanics, Solid Mechanics and its Applications*, vol. 76, pp. 29–42. Springer.
- CHARBONNEL, C. & ZAHN, J.P. 2007 Thermohaline mixing: a physical mechanism governing the photospheric composition of low-mass giants. *Astron. Astrophys.* **467** (1).
- GUILLOT, T. 1999 Interiors of Giant Planets Inside and Outside the Solar System. *Science* **286** (5437), 72.
- KRAICHNAN, R. H. 1967 Inertial ranges in two-dimensional turbulence. *Phys. Fluids* **10**, 1417–1423.
- KRISHNAMURTI, R. 2003 Double-diffusive transport in laboratory thermohaline staircases. *J. Fluid Mech.* **483**, 287–314.
- KRISHNAMURTI, R. 2009 Heat, salt and momentum transport in a laboratory thermohaline staircase. *Journal of Fluid Mechanics* **638**, 491–+.
- MERCERET, F.J. 1977 A possible manifestation of double diffusive convection in the atmosphere. *Boundary Layer Meteorol.* **11** (1), 121–123.
- MERRYFIELD, W.J. 2000 Origin of Thermohaline Staircases. *J. Phys. Oceanogr.* **30** (5), 1046–1068.
- ÖZGÖKMEN, T., ESENKOV, O. & OLSON, D. 1998 A numerical study of layer formation due to fingers in double-diffusive convection in a vertically-bounded domain. *J. Mar. Res.* **56** (2), 463–487.
- RADKO, T. 2003 A mechanism for layer formation in a double-diffusive fluid. *J. Fluid Mech.* **497**, 365–380.
- RADKO, T. 2005 What determines the thickness of layers in a thermohaline staircase? *J. Fluid Mech.* **523**, 79–98.
- RADKO, T. 2007 Mechanics of merging events for a series of layers in a stratified turbulent fluid. *J. Fluid Mech.* **577**, 251–273.
- RUDDICK, B. & GARGETT, A.E. 2003 Oceanic double-diffusion: Introduction. *Prog. Oceanogr.* **56**, 381–393.
- SCHMITT, R.W. 1979 The growth rate of super-critical salt fingers. *Deep-Sea Res.* **26A**, 23–40.
- SCHMITT, R.W. 1994 Double Diffusion in Oceanography. *Annu. Rev. Fluid Mech.* **26** (1), 255–285.
- SCHMITT, R.W., LEDWELL, J.R., MONTGOMERY, E.T., POLZIN, K.L. & TOOLE, J.M. 2005 Enhanced Diapycnal Mixing by Salt Fingers in the Thermocline of the Tropical Atlantic. *Science* **308** (5722), 685.
- STANCLIFFE, R.J., GLEBBEEK, E., IZZARD, R.G. & POLS, O.R. 2007 Carbon-enhanced metal-poor stars and thermohaline mixing. *Astron. Astrophys.* **464**, L57–L60.
- STERN, M.E. 1960 The salt fountain and thermohaline convection. *Tellus* **12** (2), 172–175.
- STERN, M.E. 1967 Lateral mixing of water masses. *Deep-Sea Res.* **14** (1), 747–753.
- STERN, M.E. 1969 Collective instability of salt fingers. *J. Fluid Mech.* **35**.
- STERN, M.E., RADKO, T. & SIMEONOV, J. 2001 Salt fingers in an unbounded thermocline. *J. Mar. Res.* **59** (3), 355–390.

- STERN, M.E. & TURNER, J.S. 1969 Salt fingers and convecting layers. *Deep-Sea Res.* **16** (1), 97–511.
- TAIT, R.I. & HOWE, M.R. 1971 Thermohaline staircase. *Nature* **231** (5299), 178–179.
- TAIT, S. & JAUPART, C. 1989 Compositional convection in viscous melts. *Nature* **338** (6216), 571–574.
- TOOLE, J. & GEORGI, D. 1981 On the dynamics of double diffusively driven intrusions. *Prog. Oceanogr.* **10**, 123–145.
- VAUCLAIR, S. 2004 Metallic Fingers and Metallicity Excess in Exoplanets’ Host Stars: The Accretion Hypothesis Revisited. *Astrophys. J.* **605** (2), 874–879.
- VERONIS, G. 2007 Updated estimate of double diffusive fluxes in the C-SALT region. *Deep-Sea Res. I* **54**.
- WALSH, D. & RUDDICK, B. 1995 Double-diffusive interleaving: The influence of nonconstant diffusivities. *J. Phys. Oceanogr.* **25**, 348–358.